

An Orthopyroxene Structure Up to 850°C

JOSEPH R. SMYTH¹

Department of Geological Sciences, Harvard University,
Cambridge, Massachusetts 02138

Abstract

Single-crystal X-ray intensity data have been obtained from a crystal of ferrohypersthene, $\text{Mg}_{0.30}\text{Fe}_{0.68}\text{Ca}_{0.015}\text{SiO}_3$, at 20°, 175°, 280°, 500°, 700°, and 850°C. Refinements of the crystal structure using three dimensional data and anisotropic thermal models have been made at each temperature. Precession photographs indicate that the space group remains *Pbca* up to 1000°. The thermal expansions of three cell edges are nearly equal and form smooth curves concave upwards. The changes in the structure with increasing temperature are largely due to the great difference between the expansion rates of *T*-O and *M*-O bonds. The silicon-oxygen (*T*-O) distances show a zero or slightly negative expansion while the *M*1- and *M*2-oxygen distances show expansions of approximately 0.25 percent per hundred degrees C. The difference in expansion rates causes the kinked silicate chains to straighten out, increasing the coordination of *M*2 from six to seven. The resulting coordination polyhedron of *M*2 at 850°C is significantly larger than that of *M*2 in high clinopyroxene of the same composition.

Introduction

Orthopyroxene is a mineral of great mineralogic and geophysical interest and importance. It is a major constituent of mafic igneous and metamorphic rocks and has been postulated as a major constituent of the earth's upper mantle. A knowledge of the structure at high temperature will permit calculation and understanding of optical absorption spectra, as well as answer many questions about the high temperature crystal chemistry of silicates in general and pyroxenes in particular.

In the pyroxene quadrilateral (MgSiO_3 - FeSiO_3 - $\text{FeCaSi}_2\text{O}_6$ - $\text{MgCaSi}_2\text{O}_6$), the orthopyroxene structure (space group *Pbca*) occurs naturally for compositions ranging from pure MgSiO_3 to $\text{Mg}_{0.12}\text{Fe}_{0.88}\text{SiO}_3$ with generally less than three mole percent CaSiO_3 . The structure is stable at 20°C over geologic time and in the composition range Fs_{50} to Fs_{80} has been observed to invert reconstructively to a monoclinic form above 950°C. The monoclinic form occurs with space group *P*2₁/*c* at 20°C and undergoes a displacive inversion to space group *C*2/*c* on heating (Smyth, 1969; Prewitt, Papike, and Ross, 1970). In the *C*2/*c* structure (as determined by Brown *et al.*, 1972; Smyth and Burn-

ham, 1972; and Ohashi, 1972), the two silicate chains, which are crystallographically distinct in orthopyroxene and primitive clinopyroxene, become symmetrically related by *C*-centering. Because the topology of the two chains in orthopyroxene is different, a similar displacive increase in symmetry with temperature is not possible in that structure. That is, the highest topologic symmetry (as defined by Smith, 1970) of orthopyroxene is *Pbca*. Precession photographs taken of orthopyroxene at 950°C confirm the space group, but they also show strong changes in the intensities of several reflections with increasing temperature, indicating significant changes of atomic positions. A detailed study of the structure of an orthopyroxene as a function of temperature was undertaken to compare its behavior with that of a primitive clinopyroxene of the same composition (Smyth and Burnham, 1972) and also to provide insight into the high temperature crystal chemistry of silicates in general.

Experimental

The clinopyroxene studied by Smyth and Burnham (1972) was formed by transformation from a natural orthopyroxene of approximate composition $\text{Fs}_{70}\text{En}_{30}$. For direct comparison, the same orthopyroxene was used for the current study. Improved single-crystal mounting and heating methods have

¹ Present address: Lunar Science Institute, 3303 Nasa Road 1, Houston, Texas 77058.

recently been developed and described in detail (Smyth, 1972). The heating device was used on a Picker automated diffractometer and allowed temperatures up to 1000°C to be maintained $\pm 10^\circ$ for a period of time long enough to make over 1000 measurements of integrated intensities of X-ray reflections.

A roughly prismatic single cleavage fragment (approx. $0.25 \times 0.40 \times 0.75$ mm) which was free of visible inclusions and exsolution lamellae was selected for study. The crystal was mounted in an evacuated silica-glass capillary which had been flushed out with H₂ gas. Using Nb-filtered Mo radiation and 2θ scans, 1849 non-equivalent integrated intensities were measured at room temperature. This represents all symmetry-independent reflections with a 2θ of less than 70° . The crystal was then heated to $175 \pm 10^\circ\text{C}$ for 12 hours before intensity measurement began again. Within 36 hours 947 non-equivalent intensities were remeasured, representing all symmetry-independent reflections with 2θ less than 50° . Similar procedures were employed at 280° and 500°C . Details of the intensity measurements are presented in Table 1.

Virgo and Hafner (1969) report that Mg and Fe begin to disorder in the *M1* and *M2* sites at about 500°C , and that at that temperature, equilibrium is reached after about 50 hours. In order to check the establishment of equilibrium with respect to the Mg, Fe distribution, the crystal was quenched after the 500°C data were collected, and a new set of data was taken at room temperature.

At 700°C , Virgo and Hafner report that Mg-Fe distribution equilibrium should be easily reached within 24 hours. The crystal was heated to 700° and allowed to equilibrate for 24 hours before the sixth

TABLE 1. Details of Intensity Measurements and Refinements

Temperature ($^\circ\text{C} \pm 10^\circ\text{C}$)	8	175	280	500	700	850
Crystal #	1	1	1	1	1	2
Radiation	MoK	MoK	MoK	MoK	MoK	MoK
Filter	Nb	Nb	Nb	Nb	Nb	Nb
Take-off angle ($^\circ$)	3.0	3.0	3.0	3.0	3.0	3.0
KV / MA	36/16	36/16	36/16	36/16	36/16	36/16
2θ scan speed ($^\circ/\text{min.}$)	1.0	2.0	2.0	2.0	2.0	2.0
Maximum 2θ ($^\circ$)	70	50	50	50	50	50
Number of measurements	1849	947	951	960	965	967
Number of observed reflections	1217	650	641	623	602	606
Final weighted R	0.046	0.049	0.049	0.057	0.056	0.086

set of X-ray intensity measurements was begun. All symmetry-independent intensities with 2θ less than 50° were measured, and the crystal was then heated to 850°C and allowed to equilibrate for 24 hours. During the intensity measurements at 850°C , the capillary was accidentally ruptured and the crystal oxidized. A new crystal was mounted and heated to 850°C and allowed to equilibrate for 24 hours. A similar sphere of X-ray intensities was measured at 850°C using the second crystal.

Before and after each data collection, cell dimensions were calculated from precise centering of three reflections on the Picker automated diffractometer. The three reflections were chosen to represent an approximately orthogonal set of reciprocal lattice vectors, each with a 2θ greater than 40° . The average of the two measurements at each temperature is presented in Table 2. The non-systematic error in each measurement was estimated from the repeatability of such determinations. Figure 1 is a plot of the normalized cell dimensions as a function of

TABLE 2. Cell Dimensions at Various Temperatures

Method	Back Reflection Weissenberg		Diffractometer					
	20	20 (after heating to 900°C)	20	175	280	500	700	850
a (Å)	18.363(5) ¹	18.377(6)	18.337	18.364	18.371	18.429	18.483	18.546
b (Å)	8.990(3)	8.996(3)	8.971	8.988	9.000	9.028	9.053	9.081
c (Å)	5.232(4)	5.233(6)	5.232	5.238	5.242	5.260	5.280	5.298
V (Å ³)	863.7(5)	865.1(5)	860.7	864.9	866.7	875.1	883.5	892.3

¹ Parenthesized figures represent the estimated standard deviation (*esd*) in terms of least units for the value to their immediate left, thus 18.363(5) indicates an *esd* of 0.005. This notation for *esd* is used consistently throughout this work.

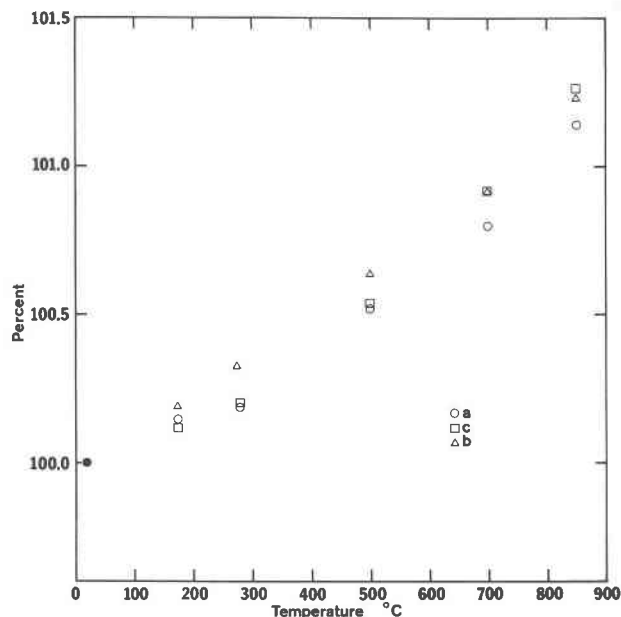


FIG. 1. Normalized linear thermal expansion of the three crystallographic axes of B1-9 orthopyroxene.

temperature. It can be seen from the figure that all curves are smooth and concave upwards, and that all crystallographic directions have nearly equal percentage thermal expansion coefficients. While the relative values of these parameters are fairly reliable, there is some systematic error in cell dimensions due largely to absorption effects. Precision back-reflection Weissenberg photographs at 20°C were taken using filtered Cu radiation of two crystals, one unheated and one heated at 900°C for 24 hours. Thirty-five lattice spacings in the range $110^\circ < 2\theta < 165^\circ$ were measured for each crystal. Cell dimensions were refined along with correction terms for absorption, film shrinkage, and camera eccentricity using the least-squares program LCLSQ (Burnham, 1966). Cell dimensions with standard errors from these refinements are presented in Table 2 along with dimensions obtained directly from the diffractometer.

Refinements

All sets of integrated intensities were corrected for Lorentz and polarization effects. Each intensity measurement was also corrected for absorption differences using numerical integration techniques (Burnham, 1966). Based on a linear absorption coefficient of 54.7 cm^{-1} , the transmission factors varied from 0.33 to 0.51 for the first crystal and 0.22 to 0.46 for the second. All refinements of the

structure models were done with a version of the full-matrix least-squares refinement program RFINE (Finger, 1969) modified for handling disk files on IBM 360 and 370 computers. All observations were weighted according to $\omega = 1/\sigma_F^2$ where σ_F is the standard deviation based on counting statistics as described by Burnham *et al* (1971). All observations below the minimum observable level (2σ) were rejected from the normal equations matrix during refinement of the model. Atomic scattering factors used are those given by Cromer and Mann (1968) for half ionized atoms as derived from Hartree-Fock wave functions neglecting relativistic effects. In addition, both real and imaginary anomalous dispersion terms (*International Tables for X-ray Crystallography*, Vol. 3, p. 215) were included in the final two cycles of refinement at each temperature. Throughout initial refinements, the chemistry was constrained to that given by Virgo and Hafner (1969).

The initial structure model used in the room temperature refinement was that given by Burnham *et al* (1971) for an orthopyroxene of approximate composition $\text{Fs}_{85}\text{En}_{12}\text{Wo}_3$. Four cycles of least squares refinement of atomic coordinates and isotropic temperature factors reduced the *R* value from 0.167 to 0.060. Two additional cycles of refinement of atomic coordinates, anisotropic temperature factors, and Mg, Fe distribution over *M1* and *M2*, including anomalous dispersion terms, gave a further reduction of the weighted *R* to 0.046. The atomic coordinates at equivalent isotropic temperature factors obtained from this final cycle were then used as the initial model for refinement of the structure at 175°C. Two cycles of least squares refinement with isotropic temperature factors, followed by two

TABLE 3. Chemical Composition Determined by Electron Microprobe

Oxide	Weight percent	Cation	Ratios based on 6 oxygens
MgO	10.51	Mg	0.636
FeO	39.10	Fe	1.327
CaO	0.73	Ca	0.032
TiO ₂	0.07	Ti	0.002
Al ₂ O ₃	0.10	Al	0.005
SiO ₂	49.19	Si	1.997
Total	99.70		3.999

TABLE 4. Occupancies, Fractional Coordinates, and Isotropic Temperature Factors for Orthopyroxene at Several Temperatures

Atom	20°C	175°C	280°C	500°C	700°C	850°C	20° (after 500°)	
M1	Mg Occ.	0.574(3)	0.596(4)	0.594(4)	0.576(5)	0.512(5)	0.553(5)	
	Fe Occ.	0.425(3)	0.403(4)	0.406(4)	0.423(5)	0.488(5)	0.447(5)	
	X	0.37546(5)	0.3754(1)	0.3753(1)	0.3752(1)	0.3746(6)	0.3746(6)	0.3756(1)
	Y	0.65459(9)	0.6543(2)	0.6540(2)	0.6532(2)	0.6520(2)	0.6514(7)	0.6546(2)
	Z	0.87652(18)	0.8783(3)	0.8799(4)	0.8841(4)	0.8879(5)	0.8919(14)	0.8760(3)
B	0.54(3)	0.79(5)	1.01(6)	1.46(7)	1.88(7)	2.67(18)	0.66(6)	
M2	Mg Occ.	0.062(3)	0.039(4)	0.042(4)	0.059(5)	0.124(5)	0.143(16)	0.083(5)
	Fe Occ.	0.906(3)	0.929(4)	0.925(4)	0.909(5)	0.844(5)	0.825(16)	0.885(5)
	Ca Occ.	0.032(F) ¹	0.032(F)	0.032(F)	0.032(F)	0.032(F)	0.032(F)	0.032(F)
	X	0.37779(4)	0.3777(1)	0.3776(1)	0.3772(1)	0.3769(1)	0.3767(5)	0.3778(1)
	Y	0.48398(6)	0.4844(1)	0.4848(1)	0.4850(2)	0.4860(2)	0.4856(6)	0.4841(1)
Z	0.36943(13)	0.3715(2)	0.3738(2)	0.3777(3)	0.3832(4)	0.3905(12)	0.3691(2)	
B	0.61(2)	1.11(4)	1.39(4)	1.99(5)	2.71(7)	3.55(17)	0.66(4)	
SiA	X	0.27182(6)	0.2719(1)	0.2720(1)	0.2719(1)	0.2723(2)	0.2720(9)	0.2717(1)
	Y	0.33967(13)	0.3399(2)	0.3394(3)	0.3392(3)	0.3389(4)	0.3389(13)	0.3400(2)
	Z	0.05188(22)	0.0531(4)	0.0542(4)	0.0572(5)	0.0604(5)	0.0644(16)	0.0510(4)
	B	0.50(4)	0.84(7)	1.00(7)	1.34(7)	1.64(8)	2.41(19)	0.66(6)
SiB	X	0.47391(6)	0.4740(1)	0.4741(1)	0.4745(2)	0.4749(2)	0.4750(9)	0.4738(1)
	Y	0.33560(13)	0.3356(3)	0.3358(3)	0.3362(3)	0.3365(4)	0.3372(13)	0.3356(2)
	Z	0.79182(22)	0.7917(4)	0.7907(4)	0.7874(5)	0.7833(6)	0.7784(17)	0.7922(4)
	B	0.47(4)	0.85(7)	1.02(7)	1.33(7)	1.74(8)	2.41(19)	0.60(6)
O1A	X	0.1838(2)	0.1834(3)	0.1832(3)	0.1841(4)	0.1841(4)	0.1841(18)	0.1841(2)
	Y	0.3376(2)	0.3374(6)	0.3376(6)	0.3377(7)	0.3377(9)	0.3374(30)	0.3381(5)
	Z	0.0441(6)	0.0454(9)	0.0476(10)	0.0522(12)	0.0578(12)	0.0550(42)	0.0419(9)
	B	0.52(9)	0.86(17)	1.01(18)	1.29(19)	1.84(21)	4.17(58)	0.53(15)
O2A	X	0.3113(2)	0.3114(3)	0.3116(3)	0.3120(4)	0.3124(4)	0.3126(15)	0.3111(3)
	Y	0.4991(3)	0.4980(6)	0.4967(6)	0.4952(7)	0.4945(9)	0.4950(25)	0.4988(6)
	Z	0.0570(5)	0.0616(9)	0.0634(10)	0.0684(12)	0.0730(14)	0.0773(39)	0.0580(9)
	B	0.72(9)	1.03(18)	1.32(19)	1.87(20)	2.36(22)	3.13(51)	0.95(16)
O3A	X	0.3023(2)	0.3025(3)	0.3024(3)	0.3019(4)	0.3007(4)	0.2987(17)	0.3024(3)
	Y	0.2347(3)	0.2353(6)	0.2367(6)	0.2374(8)	0.2380(9)	0.2394(22)	0.2338(6)
	Z	-0.1790(6)	-0.1807(11)	-0.1805(12)	-0.1778(14)	-0.1765(17)	-0.1724(40)	-0.1793(11)
	B	0.69(9)	1.36(18)	1.53(19)	2.22(21)	2.83(24)	3.11(51)	0.95(16)
O1B	X	0.5623(2)	0.5623(3)	0.5624(3)	0.5627(3)	0.5617(4)	0.5621(18)	0.5621(3)
	Y	0.3361(3)	0.3363(6)	0.3366(6)	0.3384(7)	0.3400(9)	0.3410(29)	0.3354(6)
	Z	0.7910(5)	0.7879(10)	0.7867(10)	0.7859(12)	0.7810(13)	0.7746(42)	0.7924(9)
	B	0.54(9)	0.95(17)	1.16(19)	1.55(19)	1.96(22)	4.14(56)	0.75(15)
O2B	X	0.4340(2)	0.4341(3)	0.4342(3)	0.4345(4)	0.4345(4)	0.4348(15)	0.4341(3)
	Y	0.4842(3)	0.4847(6)	0.4845(6)	0.4831(7)	0.4843(9)	0.4844(25)	0.4838(6)
	Z	0.6965(6)	0.6994(10)	0.6997(10)	0.7031(12)	0.7045(14)	0.7133(39)	0.6981(9)
	B	0.68(9)	0.99(18)	1.07(20)	1.60(20)	2.34(23)	3.08(53)	0.68(16)
O3B	X	0.4475(2)	0.4477(3)	0.4477(3)	0.4481(4)	0.4494(4)	0.4504(17)	0.4478(3)
	Y	0.2034(3)	0.2043(5)	0.2059(5)	0.2112(7)	0.2152(9)	0.2228(24)	0.2037(5)
	Z	0.5880(6)	0.5858(11)	0.5831(12)	0.5757(14)	0.5672(16)	0.5529(41)	0.5889(11)
	B	0.64(10)	1.16(20)	1.35(21)	1.99(21)	2.61(23)	3.49(55)	0.96(17)

¹Fixed

cycles with anisotropic temperature factors and anomalous dispersion terms, yielded a final R of 0.049. The structure at each successive temperature was refined from the previous structure in a similar manner. The refinement of the structure at room temperature yielded a negative occupancy of Mg in $M2$, indicating a possible error in the chemical composition. Several crystals of sample B1-9 were analyzed on an electron microprobe with the aid of Dr. David Walker. The results of this analysis, presented in Table 3, indicate a significant amount of Ca which was not reported in the analysis by Virgo and Hafner. All structures were re-refined on the basis of the new analysis and yielded more reasonable positive occupancies of Mg in $M2$.

Final weighted R factors for each refinement are

presented in Table 1. The set of intensity data taken at room temperature after cooling from 500°C was also used for a least-squares refinement using the original room temperature structure as an initial model. Fractional atomic coordinates, isotropic temperature factors, and Fe, Mg, and Ca occupancies of $M1$ and $M2$ for refinements at each temperature are presented in Table 4. Observed and calculated structure factors for the final cycle of refinement at each temperature are available in Table 5.²

² To obtain a copy of Table 5, order NAPS Document No. 02125, by remitting in advance \$1.50 for microfiche or \$5.00 for photocopies, payable to Microfiche Publications, 305 East 46th Street, New York, N. Y. 10017. Please check the most recent issue of this journal for the current address and prices.

Discussion

The room temperature structure refinement provides some valuable additional information about the crystal chemistry of orthopyroxenes. As opposed to the suggestion by Morimoto and Koto (1969), the average $M1-O$ distances do appear to vary linearly with the Fe occupancy of the $M1$ site. Figure 2 is a plot of the mean $M-O$ distances versus Fe occupancy for several modern refinements of orthopyroxene structures low in Al. The average $M1-O$ distance for aluminous orthopyroxene (Takeda, 1972) plots below the line in Figure 2. Interestingly, the average $M1-O$ distance for primitive clinopyroxene of the same composition (Smyth and Burnham, 1972) also plots on this line.

The $M2-O$ distances show no such nice linearity for several reasons. First, the Ca-content of $M2$ is quite variable and, even in small quantities, has a significant effect on the $M2-O$ distances. Second, the bond strengths of the various oxygens surrounding $M2$ are much more variable than those about $M1$ as demonstrated by the variability in distances. Third, there are no modern refinements of an orthopyroxene with an Mg occupancy of $M2$ in the 10 to 80 percent range.

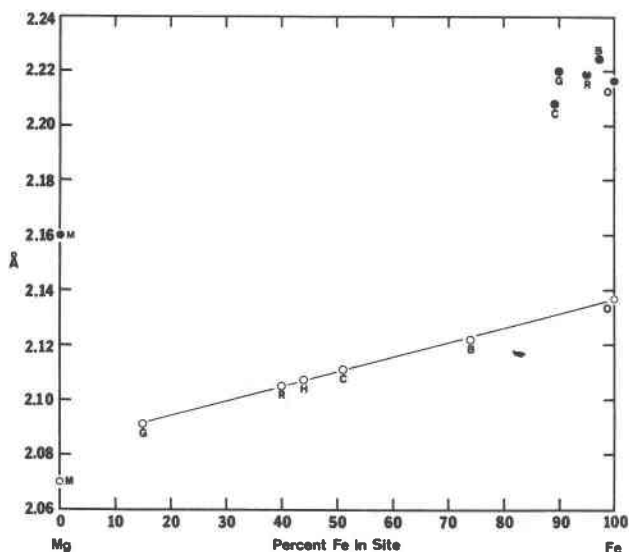


FIG. 2. Variation of mean $M-O$ bond distance with Fe occupancy of $M1$ and $M2$ sites in orthopyroxenes at room temperature. Symbols: M, enstatite (Morimoto & Koto, 1969); G, hypersthene (Ghose, 1965); R, ferrohypersthene unheated; H, ferrohypersthene, heated to 500° 48 hours; C, clinohypersthene (Smyth and Burnham, 1972); B, eulite (Burnham, *et al*, 1971); O, orthoferrosilite (Burnham, personal communication); open figures, $M1$; solid, $M2$.

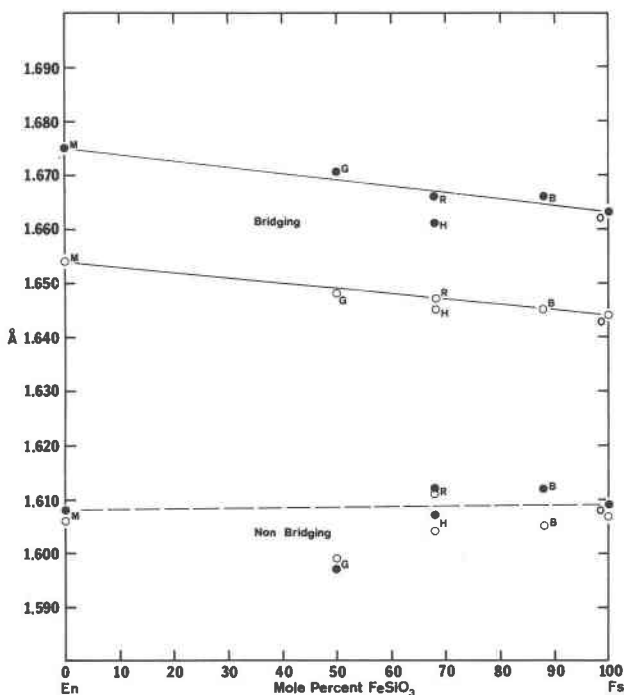


FIG. 3. Variation of the mean bridging and non-bridging Si-O distances with bulk composition of orthopyroxene. Open circles are mean Si_A-O distances, solid are mean Si_B-O distances. References and identification are the same as those for Figure 2.

Morimoto and Koto (1969) suggest that the Si-O distances vary linearly with the Fe/Fe + Mg ratio of the whole crystal. As can be seen in Figure 3, the initial room temperature structure refinement strongly supports the conclusion for the bridging oxygens. However, the linear relationship does not appear to be quite as good for the non-bridging oxygens. The refinement done at $20^\circ C$ after cooling from 500° shows a slight general decrease in Si-O distances of about 2σ over the initial refinement. It may be that the linear relationship is most applicable for highly ordered orthopyroxenes or that thermal history has some other effect on Si-O distances. More refinements of heated orthopyroxenes are needed before any firm conclusion can be drawn concerning the effects of thermal history.

The series of refinements at elevated temperatures yields much insight into the high temperature behavior of silicates in general and the structure of orthopyroxene in particular. Table 6 contains the distances between the centroids of vibration of the various cations and their nearest neighbor oxygens obtained directly from the final cycle of refinement at each temperature. In addition to the disordering

TABLE 6. Selected Interatomic Distances (Uncorrected) and Angles

ATOMS	20°	175°	280°	500°	700°	850°	20° After 500°C
SiA - O1A	1.615(2)	1.623(3)	1.632(3)	1.617(3)	1.631(3)	1.630(5)	1.608(2)
- O2A	1.606(2)	1.597(3)	1.592(3)	1.592(3)	1.593(3)	1.607(5)	1.599(2)
- O3A	1.657(2)	1.648(3)	1.648(3)	1.652(4)	1.640(4)	1.642(6)	1.658(2)
- O3A'	1.633(2)	1.638(3)	1.638(3)	1.637(4)	1.635(4)	1.624(6)	1.636(2)
Average of 4	1.628	1.628	1.628	1.625	1.625	1.625	1.625
O3A-O3A-O3A Angle	167.2°	168.5°	169.5°	170.1°	170.5°	172.1°	167.3°
SiB - O1B	1.620(2)	1.621(3)	1.621(3)	1.626(3)	1.604(4)	1.615(5)	1.618(2)
- O2B	1.603(2)	1.603(3)	1.599(3)	1.581(3)	1.588(3)	1.570(5)	1.595(2)
- O3B	1.669(2)	1.670(3)	1.669(3)	1.657(4)	1.652(4)	1.649(6)	1.662(2)
- O3B'	1.663(2)	1.653(3)	1.651(3)	1.649(4)	1.640(4)	1.619(6)	1.662(2)
Average of 4	1.639	1.637	1.635	1.628	1.621	1.613	1.634
O3B-O3B-O3B Angle	144.5°	145.1°	146.3°	150.2°	153.2°	159.3°	144.7°
Average Bridging	1.656	1.653	1.652	1.649	1.642	1.634	1.655
Average Non-Bridging	1.611	1.611	1.611	1.604	1.604	1.605	1.605
Average All	1.633	1.632	1.631	1.626	1.623	1.620	1.630
M1 - O1A	2.158(2)	2.155(3)	2.157(3)	2.179(3)	2.197(4)	2.189(6)	2.161(3)
- O1A'	2.054(2)	2.053(3)	2.048(3)	2.062(3)	2.060(4)	2.094(6)	2.064(3)
- O2A	2.057(2)	2.068(3)	2.073(3)	2.081(3)	2.081(4)	2.075(6)	2.065(3)
- O1B	2.084(2)	2.091(3)	2.091(3)	2.080(3)	2.104(4)	2.122(6)	2.079(3)
- O1B'	2.176(2)	2.178(3)	2.185(3)	2.214(3)	2.248(4)	2.262(6)	2.172(3)
- O2B	2.094(2)	2.089(3)	2.095(3)	2.111(3)	2.109(4)	2.106(6)	2.089(3)
Average of 6	2.104	2.106	2.108	2.121	2.133	2.141	2.105
M2 - O1A	2.165(2)	2.158(3)	2.152(3)	2.164(4)	2.160(4)	2.147(6)	2.157(3)
- O1B	2.129(2)	2.124(3)	2.124(3)	2.123(4)	2.126(4)	2.128(6)	2.135(3)
- O2A	2.045(2)	2.033(3)	2.032(3)	2.025(4)	2.026(4)	2.043(6)	2.039(3)
- O2B	1.999(2)	2.005(3)	2.000(3)	2.011(4)	2.003(4)	2.022(6)	2.007(3)
- O3A	2.417(2)	2.425(4)	2.442(4)	2.458(4)	2.488(4)	2.525(8)	2.408(3)
- O3B	2.577(2)	2.602(4)	2.632(4)	2.715(4)	2.810(4)	2.943(8)	2.576(3)
- O3B'	3.050(2)	3.042(4)	3.027(4)	2.984(4)	2.958(4)	2.881(8)	3.051(3)
Average of First 4	2.085	2.080	2.077	2.081	2.079	2.085	2.085
Average of First 6	2.222	2.225	2.230	2.249	2.268	2.301	2.222
Average of 7	2.340	2.341	2.344	2.354	2.367	2.384	2.339

of Fe and Mg over the *M*-sites, we can see in Table 6 three major effects of temperature on the bond distances and angles. These effects are: one, the large expansion of the *M*-O distances; two, the zero or slightly negative expansion of the *T*-O distances; and three, the straightening of the silicate chains caused by the great difference in the expansions of the *M*-O and *T*-O distances. The very significant difference between the *M*-O and *T*-O distances is clearly demonstrated in Figure 4 and the chain angles versus temperature are plotted in Figure 5.

Refinement of the structural coordinates from X-ray intensity data gives the positions of the centroids of the ellipsoid describing the thermal motion of each atom. In order to calculate the time-averaged mean separation between atom centers which will be somewhat larger than the distances in Table 6, it is necessary to have a rigorous dynamic description of the crystal, which is not currently possible. We can, however, make a fair estimate of the true interatomic distances. Busing and Levy (1964) present four models for correcting the centroid distances for

thermal motion, which are incorporated into the refinement and errors programs (RFINE and BADTEA, L. W. Finger, 1969). The corrections become significant as the amplitude of thermal vibration exceeds 0.10Å. Two of the models place lower and upper bounds on the correction terms by assuming, respectively, highly correlated parallel and anti-parallel displacements of the atoms from the centroids. Within these limits are two, more realistic, correction models. The first of these considers the vector of separation between the atoms to be independent of the position of one of the atoms. This is the riding correction and is most applicable to strongly bonded atoms such as those in molecular crystals in which groups of atoms vibrate as a rigid body. The second is the non-correlated correction which assumes that the atoms vibrate completely independently of one another. This model results in a larger correction term than the riding model and is most applicable to weakly bonded atoms. In a complex silicate, neither model is rigorously applicable, but the true mean separation of atom centers

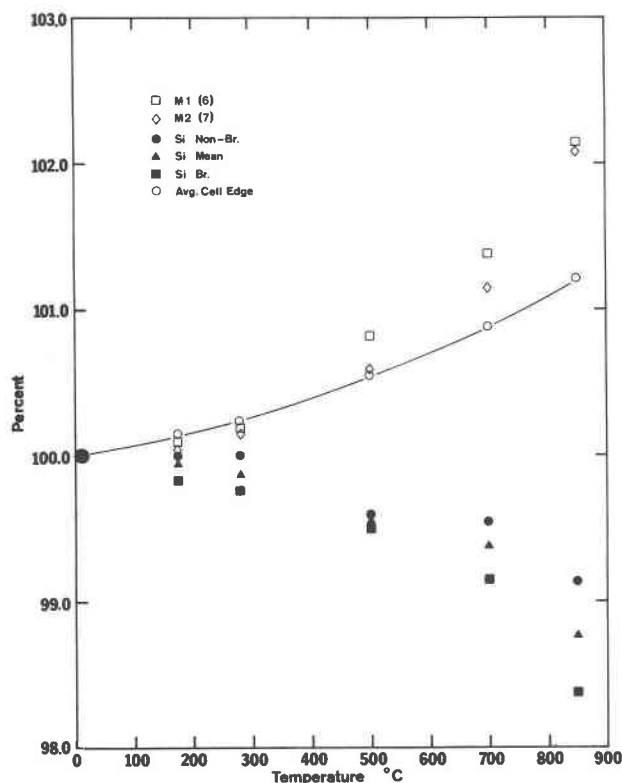


FIG. 4. Variation of the mean separation of the centroids of thermal motion with temperature for *M* and *T* cations and their surrounding oxygens. Distances are plotted as a percent of their initial value at 20°C.

should lie somewhere between the riding and non-correlated corrections. The riding correction should be more applicable to the strong silicon-oxygen bonds whereas the non-correlated correction should be more applicable to the *M*-O bonds. Bond distances in Table 7 are corrected for riding motion while those of Table 8 are corrected assuming non-correlated thermal motion.

A simple ionic bonding model can help to explain the major effects of temperature on this structure. Expansion of the cation-oxygen bond length with increasing temperature appears to vary inversely with the ionic strength of the bond. Weaker bonds have lower frequencies of thermal vibration, hence lower energies of excitation, and therefore are the first to be excited with increasing temperature. The decreased bond strength to oxygen of the *M*-cations is balanced by an increased bond strength to silicon, hence the net decrease in the separation of the silicon and oxygen centroids of motion. An increase in the *M*-O distances coupled with a decrease in the *T*-O distances forces the kinked chains of tetrahedra to

straighten. Looking in detail at the behavior of the various coordination polyhedra, we can see some of the consequences of these principles.

The *M1* site is occupied by a divalent cation, Mg or Fe. It is surrounded by six oxygens (two O1A, two O1B, one O2A, and one O2B) forming a nearly regular octahedron although the point symmetry of the site is 1. Each of the six-bonds to oxygens may be assigned a Pauling bond strength of 0.33. It can be seen from Table 6 of bond lengths that each bond shows a roughly equal positive expansion increasing by about two percent at 850° over its room temperature value. When the distances are corrected for thermal motion, the expansions are even larger. The curve of the averaged bond distances versus temperature (Figure 4) is concave upwards. The bonds showing the least expansion are those to O2A and O2B, the undersaturated oxygens, the strongest bonds in the coordination polyhedron.

The *M2* site, occupied by divalent cations, Mg and Fe, but also in this case by Ca, is an irregular site which changes coordination number with increasing temperature. The coordination of the *M2* site has generally been considered to be six-fold,

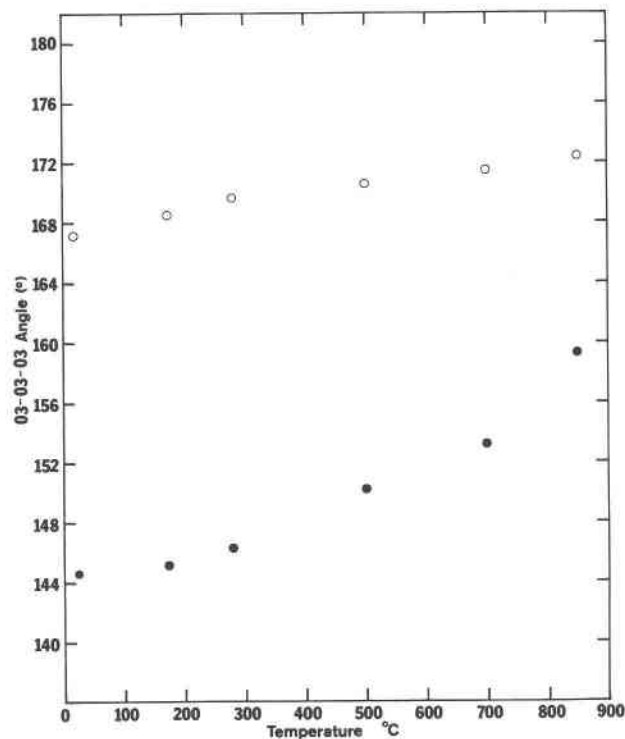


FIG. 5. Variation of O3-O3-O3 chain-axis angle of A and B chains in orthopyroxene with temperature. Solid circles represent B-chain; open, A-chain.

TABLE 7. Selected Interatomic Distances Corrected for Riding Motion

ATOMS	20°	175°	280°	500°	700°	850°
SiA-O1A	1.615	1.624	1.632	1.618	1.632	1.644
O2A	1.608	1.597	1.594	1.595	1.597	1.615
O3A	1.658	1.653	1.653	1.660	1.652	1.648
O3A'	1.635	1.645	1.639	1.640	1.639	1.634
Avg. of 4	1.629	1.630	1.630	1.628	1.630	1.635
SiB-O1B	1.621	1.622	1.622	1.627	1.604	1.628
O2B	1.604	1.603	1.601	1.582	1.593	1.576
O3B	1.671	1.673	1.673	1.664	1.660	1.656
O3B'	1.664	1.654	1.652	1.652	1.645	1.624
Avg. of 4	1.640	1.638	1.637	1.631	1.626	1.621
Avg. of 8	1.635	1.634	1.633	1.630	1.628	1.628
M1-O1A	2.158	2.155	2.157	2.180	2.198	2.193
O1A'	2.054	2.053	2.048	2.062	2.060	2.099
O1B	2.085	2.093	2.093	2.081	2.104	2.139
O1B'	2.176	2.178	2.186	2.214	2.249	2.269
O2A	2.058	2.069	2.073	2.082	2.083	2.080
O2B	2.095	2.091	2.098	2.113	2.114	2.106
Avg. of 6	2.104	2.107	2.109	2.122	2.135	2.148
M2-O1A	2.164	2.158	2.154	2.166	2.165	2.147
O1B	2.129	2.125	2.125	2.126	2.131	2.130
O2A	2.045	2.034	2.034	2.029	2.032	2.051
O2B	2.000	2.007	2.004	2.016	2.010	2.036
O3A	2.418	2.427	2.443	2.460	2.488	2.526
O3B	2.578	2.603	2.632	2.716	2.812	2.943
O3B'	3.050	3.043	3.028	2.986	2.960	2.886
Avg. of 4	2.058	2.081	2.079	2.084	2.085	2.091
Avg. of 6	2.222	2.226	2.232	2.252	2.273	2.306
Avg. of 7	2.340	2.342	2.346	2.357	2.371	2.388

TABLE 8. Selected Interatomic Distances Corrected for Non-Correlated Thermal Motion

ATOMS	20°	175°	280°	500°	700°	850°
SiA-O1A	1.624	1.637	1.648	1.639	1.659	1.678
O2A	1.617	1.611	1.609	1.616	1.623	1.622
O3A	1.664	1.666	1.667	1.679	1.677	1.667
O3A'	1.643	1.658	1.654	1.661	1.665	1.643
Avg. of 4	1.637	1.643	1.645	1.649	1.656	1.653
SiB-O1B	1.629	1.635	1.637	1.648	1.632	1.663
O2B	1.612	1.616	1.614	1.603	1.620	1.589
O3B	1.677	1.686	1.688	1.684	1.687	1.681
O3B'	1.671	1.667	1.669	1.673	1.673	1.643
Avg. of 4	1.647	1.651	1.652	1.652	1.653	1.644
Avg. of 8	1.642	1.647	1.648	1.650	1.655	1.648
M1-O1A	2.164	2.164	2.167	2.194	2.216	2.211
O1A'	2.060	2.064	2.062	2.080	2.086	2.125
O1B	2.091	2.103	2.106	2.101	2.129	2.165
O1B'	2.182	2.187	2.197	2.230	2.269	2.289
O2A	2.065	2.078	2.085	2.099	2.105	2.092
O2B	2.101	2.100	2.109	2.130	2.135	2.125
Avg. of 6	2.111	2.116	2.121	2.139	2.157	2.168
M2-O1A	2.171	2.168	2.165	2.181	2.183	2.176
O1B	2.135	2.135	2.138	2.142	2.153	2.163
O2A	2.054	2.048	2.050	2.051	2.060	2.081
O2B	2.007	2.019	2.016	2.035	2.037	2.053
O3A	2.424	2.439	2.458	2.481	2.516	2.554
O3B	2.583	2.613	2.644	2.732	2.833	2.960
O3B'	3.055	3.050	3.038	2.999	2.978	2.901
Avg. of 4	2.092	2.092	2.092	2.102	2.108	2.118
Avg. of 6	2.229	2.237	2.245	2.270	2.297	2.331
Avg. of 7	2.347	2.353	2.358	2.374	2.394	2.413

however a better terminology would be four-plus-two. Four of the bonds (those to O1A, O1B, O2A, and O2B) are much shorter than those to the bridging oxygens of the silicate chains (O3A and O3B). Due to straightening of the chain at high temperature, the coordination becomes four-plus-three, with the same four short bonds but with an extra O3B coming into the coordination sphere so that there are now three long bonds. The average of the four short bonds remains nearly constant with increasing temperature while the average of all seven distances shows a strong positive expansion nearly equal to that of the mean $M1-O$ distances.

We are now faced with the question of choosing an applicable model to correct the interatomic distances for thermal motion. Certainly the riding model will not be applicable to both the $M-O$ and $T-O$ distances because the oxygens cannot ride both cations simultaneously. Because the $T-O$ bonds are much stronger than the $M-O$ bonds and the former

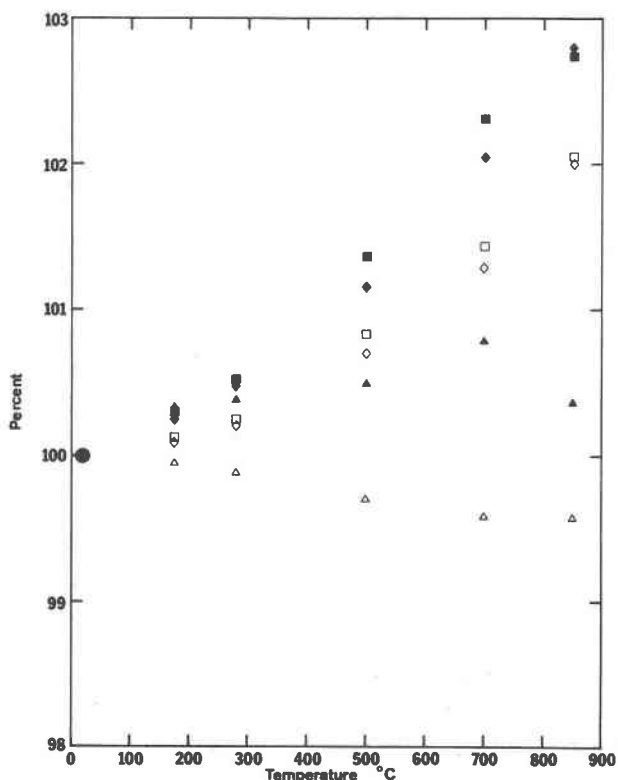


FIG. 6. Percentage variation with temperature of mean interatomic separation between cations and surrounding oxygens. Squares mean $M1-O$ distances; diamonds, $M2-O$; and triangles, $Si-O$. Open figures are corrected for riding motion; solid figures are corrected for noncorrelated thermal motion. All values are plotted as a percent of their value at 20°C.

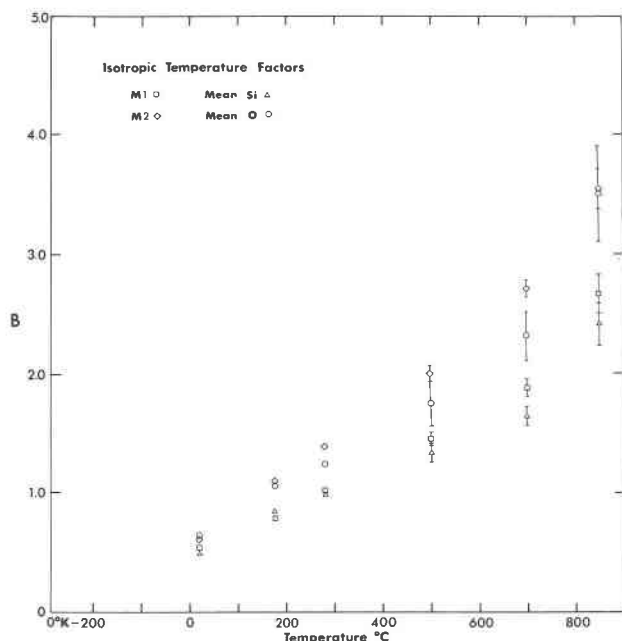


FIG. 7. Variation with temperature of isotropic temperature factors B for $M1$, $M2$, the mean Si, and mean O. Circles, $M1$; squares, $M2$; triangles, Si; diamonds, O.

change little with increasing temperature, it is reasonable to expect that the thermal motions of the oxygens will be much more strongly correlated with

Si than with the M cations. While the true mean atomic separations should lie somewhere between the two corrected values, those of the $T-O$ bonds will be closer to the riding values, while those of the $M-O$ bonds will be closer to those corrected for non-correlated thermal motion.

In marked contrast to the $M-O$ distances, the silicon-oxygen ($T-O$) bonds show a continual decrease in the separation of the centroids of motion with increasing temperature. The average of the eight tetrahedral separations decreases by about 6σ at 850°C . When a riding correction is applied to these distances, it can be seen that the average mean interatomic distance decreases by about 2σ . In looking at the individual distances, it should be noted that the shortest bonds, those to the undersaturated $O2$ atoms in both tetrahedra, show the greatest decrease. What is most important, however, is the great difference between the rates of expansion of the $T-O$ distances and the $M-O$ distances. It is this difference, a 2 to 3 percent increase in the $M-O$ distances versus a near zero increase in the $T-O$ distances, which causes the chains to straighten and the $M2$ coordination to increase from six to seven. This difference is clearly shown in Figure 6.

The temperature factors in Table 3 are equivalent

TABLE 9. Amplitudes and Orientations of Major Axes of Thermal Ellipsoids

Temperature ($^\circ\text{C}$)		20			175			280					
Atom	Axis	RMS Ampl.(\AA)	Angle/a	Angle/b	Angle/c	RMS Ampl.(\AA)	Angle/a	Angle/b	Angle/c	RMS Ampl.(\AA)	Angle/a	Angle/b	Angle/c
M1	1	0.079(1)	58(6)	100(7)	34(7)	0.093(2)	53(9)	75(10)	40(10)	0.097(2)	47(9)	87(10)	43(10)
	2	0.082(1)	112(12)	158(17)	87(10)	0.100(2)	51(15)	63(20)	130(14)	0.114(2)	47(14)	73(17)	132(14)
	3	0.086(1)	140(15)	72(16)	56(9)	0.107(2)	120(12)	31(20)	84(13)	0.125(2)	104(11)	17(18)	80(12)
M2	1	0.068(1)	42(2)	83(2)	49(2)	0.095(2)	48(4)	87(4)	42(4)	0.103(2)	45(4)	85(4)	46(5)
	2	0.093(1)	71(3)	37(4)	120(3)	0.126(2)	68(5)	33(7)	113(6)	0.140(2)	71(5)	32(8)	115(6)
	3	0.101(1)	126(3)	54(4)	56(3)	0.131(2)	130(6)	58(6)	57(6)	0.150(2)	129(5)	58(8)	55(6)
SiA	1	0.070(2)	151(6)	91(7)	61(19)	0.099(3)	0(*)	90(*)	90(14)	0.100(3)	168(14)	88(13)	79(14)
	2	0.076(2)	101(10)	155(10)	112(14)	0.100(3)	90(*)	180(*)	90(12)	0.115(3)	100(17)	132(25)	137(32)
	3	0.092(2)	63(5)	115(8)	38(9)	0.111(3)	90(10)	90(12)	0(11)	0.120(3)	84(12)	138(28)	49(30)
SiB	1	0.069(2)	18(10)	104(7)	79(11)	0.099(3)	96(17)	107(40)	18(50)	0.109(3)	86(26)	117(34)	27(32)
	2	0.077(2)	74(9)	63(10)	148(10)	0.105(3)	91(16)	164(43)	106(47)	0.112(3)	34(28)	119(33)	107(35)
	3	0.085(2)	83(6)	31(8)	60(10)	0.107(3)	6(12)	93(16)	85(14)	0.119(3)	56(29)	40(29)	70(27)
O1A	1	0.063(7)	6(14)	88(12)	85(10)	0.086(9)	80(21)	69(20)	23(19)	0.088(9)	53(22)	65(28)	47(26)
	2	0.082(7)	87(19)	173(17)	97(18)	0.110(9)	39(70)	58(75)	110(32)	0.117(9)	61(26)	62(24)	137(27)
	3	0.095(7)	95(20)	97(16)	8(15)	0.113(9)	128(71)	40(69)	101(30)	0.131(9)	129(27)	39(22)	85(24)
O2A	1	0.077(7)	111(12)	159(15)	86(14)	0.082(9)	77(20)	64(22)	29(20)	0.090(9)	107(19)	59(24)	36(19)
	2	0.098(7)	127(14)	80(16)	142(15)	0.115(9)	19(21)	82(21)	107(19)	0.132(9)	160(18)	90(22)	110(20)
	3	0.110(7)	136(16)	71(14)	52(18)	0.138(8)	76(21)	153(20)	68(22)	0.156(8)	100(20)	149(23)	61(21)
O3A	1	0.063(7)	55(18)	58(19)	51(17)	0.090(9)	148(20)	117(24)	73(21)	0.097(9)	155(20)	115(20)	88(25)
	2	0.075(7)	37(16)	100(18)	126(17)	0.126(10)	114(22)	80(23)	154(23)	0.131(10)	103(23)	66(24)	152(20)
	3	0.129(6)	78(12)	146(13)	59(14)	0.167(8)	111(22)	29(24)	71(22)	0.178(9)	111(21)	36(23)	62(22)
O1B	1	0.062(6)	23(15)	93(19)	67(17)	0.086(7)	63(20)	86(20)	27(22)	0.101(8)	59(21)	75(20)	35(22)
	2	0.082(6)	68(14)	72(14)	151(15)	0.115(8)	68(22)	157(19)	96(26)	0.125(8)	90(31)	18(31)	108(30)
	3	0.100(6)	94(17)	18(16)	73(14)	0.124(9)	114(24)	113(20)	64(24)	0.134(9)	149(33)	80(37)	61(32)
O2B	1	0.074(7)	153(13)	97(17)	64(14)	0.074(10)	130(19)	81(21)	41(21)	0.063(10)	119(19)	69(21)	37(20)
	2	0.094(7)	111(15)	39(14)	121(14)	0.119(10)	138(23)	111(25)	124(22)	0.125(11)	136(24)	133(27)	97(28)
	3	0.107(6)	74(15)	52(17)	42(16)	0.134(9)	80(24)	157(22)	70(21)	0.145(10)	60(24)	129(25)	54(25)
O3B	1	0.063(7)	46(26)	91(20)	44(27)	0.084(9)	23(21)	73(23)	76(24)	0.094(9)	19(22)	84(24)	72(20)
	2	0.070(8)	49(28)	113(19)	130(30)	0.117(9)	68(26)	126(22)	135(21)	0.133(9)	72(25)	124(25)	140(25)
	3	0.124(6)	106(15)	157(14)	75(15)	0.153(8)	86(24)	138(19)	49(21)	0.158(9)	96(26)	145(27)	56(28)

* Indicates orientation of axis is essentially indeterminate as is expected when cross section of thermal ellipsoid is nearly circular.

isotropic B 's calculated from the anisotropic temperature factors for all atoms except O1A, O2A, O2B, O3A and O3B at 850°C. The latter B 's were taken from the final cycle of isotropic refinement because the anisotropic temperature factors for these atoms were not positive-definite. Isotropic temperature factors for $M1$, $M2$, the mean for Si, and the mean for the six oxygens are plotted versus temperature in Figure 7. The temperature factors of $M1$ and $M2$ form smooth, concave-upwards curves with those of $M2$ being, in general, the largest of the structure. The relatively smaller magnitudes of the Si temperature factors may be attributed to the restrictions of strong, non-expanding bonds. The mean B for the six oxygens forms a curve similar in shape and somewhat steeper than that for Si. The similarity in shape may be due to correlated thermal motion between silicon and oxygen.

The magnitudes and orientations of the thermal ellipsoid major axes are presented in Table 9. The ellipsoids at 20°C are essentially the same as those obtained by Burnham *et al* (1971) for an orthopyroxene of approximate composition Fs_{88} . These authors conclude that "the shape of the thermal ellipsoid is governed by the configuration of the coordinating atoms and that the shortest axis, X , is

oriented parallel to the direction of the bond to the closest neighboring atom, or the longest axis, Z , is normal to that direction." This conclusion is further strengthened by the data obtained in the present work at room temperature and above.

This conclusion is clearly demonstrated in Figure 8 in which the orientations of the bonds surrounding $M1$ and $M2$ are plotted on stereo nets whose axes correspond to the principal axes of the thermal ellipsoid. In the $M1$ octahedron, the shortest distance between antipodal oxygens (O1A'-O1B) remains roughly parallel to the short axis of the ellipsoid, X , at all temperatures. The observed thermal vibration of $M2$ is much more anisotropic than $M1$ because of the greater variability of bond lengths around the former. Because of the greater anisotropy of $M2$, the correlation between bond length and the shape of the thermal ellipsoid is even more pronounced than in $M1$. The two shortest bonds around $M2$, those to O2A and O2B, are antipodal and remain parallel to the shortest axis of the thermal ellipsoid up to 850°C. At 850°, the ellipsoid undergoes a slight rotation about X so that the long axis, Z , is directed more nearly toward O3B, which has come into the coordination sphere on heating.

At room temperature, the thermal vibration of the

TABLE 9, Continued

Temperature (°C)		500				700				850			
Atom	Axis	RMS Ampl.(Å)	Angle/a	Angle/b	Angle/c	RMS Ampl.(Å)	Angle/a	Angle/b	Angle/c	RMS Ampl.(Å)	Angle/a	Angle/b	Angle/c
M1	1	0.121(2)	45(9)	81(10)	47(10)	0.136(3)	67(9)	84(10)	23(10)	0.081(10)	13(20)	85(28)	78(24)
	2	0.135(2)	47(15)	86(16)	137(14)	0.160(3)	41(24)	57(28)	112(17)	0.164(12)	79(24)	81(24)	165(25)
	3	0.150(2)	81(12)	170(15)	87(13)	0.166(3)	122(28)	33(27)	83(18)	0.198(12)	96(24)	11(21)	82(25)
M2	1	0.124(2)	51(5)	87(4)	39(5)	0.150(3)	54(6)	90(5)	36(5)	0.135(7)	41(12)	92(11)	49(11)
	2	0.166(2)	73(5)	25(7)	107(6)	0.189(3)	70(6)	25(7)	104(7)	0.204(8)	52(10)	68(12)	134(13)
	3	0.181(2)	136(6)	66(6)	56(6)	0.212(3)	138(7)	65(7)	58(7)	0.231(8)	103(11)	22(14)	72(13)
S1A	1	0.112(3)	169(14)	95(14)	81(14)	0.134(4)	17(16)	73(15)	92(15)	0.121(8)	33(31)	92(30)	57(32)
	2	0.135(4)	93(17)	136(28)	134(35)	0.142(4)	84(18)	117(20)	152(22)	0.145(8)	57(30)	93(33)	147(35)
	3	0.142(4)	80(13)	133(29)	45(33)	0.155(5)	74(16)	147(21)	62(19)	0.188(9)	93(31)	177(30)	88(37)
S1B	1	0.125(3)	115(31)	87(34)	25(38)	0.142(4)	135(41)	111(43)	52(46)	0.112(9)	6(30)	88(32)	85(28)
	2	0.130(4)	133(38)	50(41)	110(36)	0.151(4)	84(*)	154(*)	116(*)	0.149(9)	85(31)	81(29)	170(29)
	3	0.134(3)	53(35)	41(43)	76(33)	0.152(5)	48(*)	129(*)	67(*)	0.187(9)	92(31)	9(30)	81(31)
O1A	1	0.109(10)	68(28)	86(29)	22(28)	0.127(11)	75(29)	97(31)	16(30)	**			
	2	0.122(10)	24(26)	102(28)	110(29)	0.145(11)	37(30)	54(33)	98(28)				
	3	0.148(9)	99(24)	167(23)	82(23)	0.180(10)	124(35)	37(31)	76(36)				
O2A	1	0.105(10)	113(20)	38(24)	61(22)	0.126(11)	115(26)	54(24)	46(20)	**			
	2	0.159(10)	140(20)	89(24)	130(21)	0.180(12)	104(24)	48(21)	135(23)				
	3	0.186(9)	121(22)	128(21)	54(23)	0.204(12)	28(22)	63(22)	82(24)				
O3A	1	0.106(10)	155(21)	113(22)	82(22)	0.142(12)	9(26)	81(27)	87(27)	**			
	2	0.156(10)	103(25)	79(28)	163(29)	0.165(13)	91(24)	61(27)	151(27)				
	3	0.220(10)	110(24)	26(24)	75(20)	0.245(16)	99(21)	31(24)	61(25)				
O1B	1	0.109(9)	71(23)	84(25)	20(24)	0.126(12)	92(24)	77(25)	13(24)	0.137(28)	56(38)	103(36)	37(35)
	2	0.151(10)	87(*)	8(*)	97(32)	0.166(13)	111(38)	25(40)	102(28)	0.241(29)	57(40)	129(42)	123(40)
	3	0.156(10)	160(*)	84(*)	71(35)	0.175(13)	159(31)	111(37)	87(26)	0.272(32)	129(42)	138(42)	77(46)
O2B	1	0.115(11)	113(26)	72(28)	30(30)	0.141(12)	127(27)	78(30)	40(31)	**			
	2	0.143(11)	57(27)	33(26)	94(28)	0.170(13)	104(28)	30(29)	116(29)				
	3	0.165(11)	42(30)	117(29)	60(29)	0.199(13)	41(30)	63(29)	62(29)				
O3B	1	0.103(10)	17(26)	81(28)	76(28)	0.138(13)	9(26)	83(27)	84(27)	**			
	2	0.152(11)	73(28)	119(27)	145(27)	0.169(15)	82(27)	110(28)	159(28)				
	3	0.205(11)	89(26)	149(27)	59(28)	0.226(17)	85(26)	259(27)	70(27)				

** Thermal ellipsoid of this atom is not positive-definite.

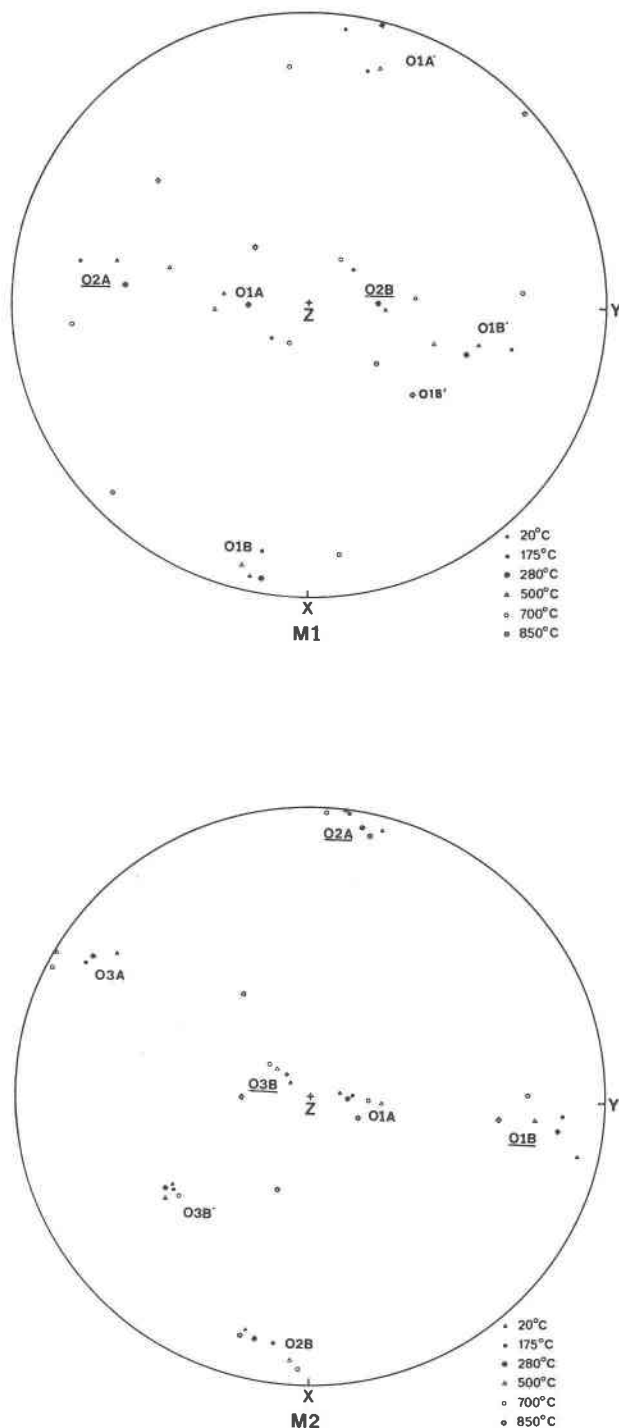


FIG. 8A, B. Stereographic (Wulff net) projection of the directions of the oxygens from the *M1* or *M2* sites they coordinate in relation to the principal axes of the apparent thermal vibration ellipsoids of *M1* and *M2* at various temperatures. *X*, *Y*, and *Z* indicate the principal axes of the ellipsoid; *Z* being the longest axis, and *X* the shortest. Underlined atom name indicates lower hemisphere plot; others are in upper hemisphere.

silicons is not strongly anisotropic although at 20°C there is a tendency for the long axes to be oriented toward the bridging oxygens. Above 700°C, the ellipsoids become prolate with long axes roughly parallel to the *b*-crystallographic axis. Such an orientation is consistent with strong libration of the silicate chain in the *b*-*c* plane.

All oxygens show a tendency to lengthen their ellipsoids in the *b* direction more than other directions, becoming prolate with long axes near *b* or oblate with their short axes near *c*. This change is also consistent with libration of the silicate chain and correlated motion of silicon and oxygen. As mentioned previously, the anisotropic temperature factors of O1A, O2A, O2B, O3A, and O3B are not positive definite at 850°C. There are several possible causes. It may be that there were insufficient data at 850° for anisotropic refinement of weak scatterers such as oxygen or some source of systematic error in the data. It may be that correlated thermal motion results in a large amplitude libration of the chain which cannot be described on the basis of a harmonic oscillator. It may be that non-correlated thermal motion of oxygens, tightly bound by non-expanding bonds to silicon in one direction and loosely bound by lengthened bonds to the *M*-cations in another direction, cannot be described as a harmonic oscillator. The true cause may be determined by better future refinements of pyroxenes at elevated temperatures.

The data on the Mg, Fe distribution in *M1* and *M2* provide a useful comparison with the work of Virgo and Hafner (1969, 1970). Although direct comparison may not be possible because these authors report no Ca in their sample of B1-9, the current X-ray refinement shows slightly more Fe in *M1* at 850° than would be expected from the Mössbauer studies. However, on the whole, agreement with Virgo and Hafner is quite good. As expected from Mössbauer studies, no disordering took place below 500°C. At 500°C equilibrium was not attained in the 24 hour heating period before data collection began, and the room temperature data taken after the 500° data indicate greater disorder of Fe and Mg than those taken at 500°C. The ΔG for the Mg-Fe exchange reaction was calculated from the equilibrium constant (Mueller, 1969) and is presented in Table 10. The constant values of ΔG for the 850°, 750°, and 20°C post 500°C refinements indicate equilibrium was probably nearly attained for these refinements. This value of ΔG

TABLE 10. *M1*, *M2* Occupancies, *K* and ΔG for Mg, Fe Exchange

Refinement Temperature (°C)	<i>M1</i>		<i>M2</i>		Ca ¹	<i>K</i>	ΔG (Kcal/mole)
	Mg	Fe	Mg	Fe			
20	0.574(3) ²	0.425	0.062	0.906	0.032		
175	0.576(4)	0.423	0.059	0.909	0.032		
280	0.574(4)	0.426	0.042	0.925	0.032		
500	0.576(5)	0.423	0.059	0.909	0.032	0.073(10)	4.01(11)
20° after 500	0.553(5)	0.447	0.083	0.885	0.032	0.109(10)	3.41(11)
700	0.512(5)	0.488	0.124	0.844	0.032	0.176(10)	3.35(11)
850	0.493(16)	0.507	0.143	0.825	0.032	0.218(30)	3.39(30)

¹ Occupancy fixed from chemical analysis.

² Parenthesized figures represent the *esd* in terms of least units cited for the value to their immediate left, thus 0.594(3) indicates an *esd* of 0.003. During refinement, each site was constrained to full occupancy and total chemistry was constrained to that given by microprobe analysis, thus all Mg, Fe occupancies at a given temperature have the same *esd*.

agrees within the standard error with those obtained by Virgo and Hafner within this temperature range.

Conclusions

It is instructive to compare the behavior of orthopyroxene with that of clinopyroxene (Smyth and Burnham, 1972) at elevated temperatures. In primitive clinopyroxene, the A-chains are S-rotated and the B-chains are O-rotated, while in orthopyroxene, both chains are O-rotated (Thompson, 1970). With increasing temperature, the primitive monoclinic structure gains symmetry by straightening the chains so that they become crystallographically equivalent. The straightening A-chains rotate through 180° (03-03-03 angle) becoming O-rotated and equivalent to the straightened B-chains. In orthopyroxene no such displacive change to gain symmetry is possible, and straightening of the silicate chains proceeds much more slowly than in clinopyroxene. Straightening of the B-chains in orthopyroxene causes the coordination of *M2* to increase from six to seven, while in clino the coordination of *M2* goes from six to seven and back to six again with a small six-coordinated *M2* site at 950°C. The inability of orthopyroxene to achieve a small six-coordinated *M2* site and the increase in symmetry at high temperature contribute to orthopyroxene's instability relative to the C-centered monoclinic structure above 950°C. Above 950°C, orthopyroxene undergoes a reconstructive inversion to high clinopyroxene (Smyth, 1969). In both ortho- and clinopyroxene, it is the

difference between the relative expansion rates of the M-O and T-O bonds which is the primary cause of chain straightening and is the major effect of temperatures on these structures.

Acknowledgment

This work was supported by National Science Foundation Grant GA 12852 through Professor C. W. Burnham at Harvard University. The author wishes to thank Professor Burnham and Dr. Hiroshi Takeda for thoughtful reading of the manuscript and helpful suggestions for its improvement. The author also thanks the Lunar Science Institute for typing and drafting services in final preparation of the manuscript.

References

- BROWN, G. E., C. T. PREWITT, J. J. PAPIKE, S. SUENO (1972) A comparison of the structures of low and high pigeonite. *J. Geophys. Res.* **77**, 5778-5789.
- BURNHAM, C. W. (1966) Computation of absorption correction and the significance of end effect. *Amer. Mineral.* **51**, 159-167.
- , Y. OHASHI, S. S. HAFNER, AND D. VIRGO (1971) Cation distribution and atomic thermal vibrations in an iron-rich orthopyroxene. *Amer. Mineral.* **56**, 850-876.
- BUSING, W. R., AND H. A. LEVY (1964) The effect of thermal motion on the estimation of bond lengths from diffraction measurements. *Acta Crystallogr.* **17**, 142-146.
- CROMER, D. T., AND J. B. MANN (1968) X-ray scattering factors computed from numerical Hartree-Fock wave functions. *Acta Crystallogr.* **24**, 321-324.
- FINGER, L. W. (1969) Determination of cation distribution by least squares refinement of single-crystal X-ray data. *Carnegie Inst. Washington Year Book*, **67**, 216-217.
- GHOSE, S. (1965) Mg²⁺-Fe²⁺ order in an orthopyroxene, Mg_{0.93}Fe_{1.07}Si₂O₆. *Z. Kristallogr.* **122**, 81-99.
- MORIMOTO, N., D. E. APPLEMAN, AND H. T. EVANS (1960) The crystal structure of clinoenstatite and pigeonite. *Z. Kristallogr.* **114**, 120-147.
- , AND K. KOTO (1969) The crystal structure of orthoenstatite. *Z. Kristallogr.* **129**, 65-83.
- MUELLER, R. F. (1969) Kinetics and thermodynamics of intracrystalline distributions. *Mineral. Soc. Amer. Spec. Pap.* **2**, 83-93.
- OHASHI, Y. (1972) *High Temperature Structural Crystallography of Synthetic Clinopyroxenes, (Ca,Fe) SiO₃*. Ph.D. Thesis, Harvard University, Cambridge, Massachusetts.
- PREWITT, C. T., J. J. PAPIKE, AND M. ROSS (1970) Cumingtonite: a reversible, nonquenchable transition from P2₁/m to C2/m symmetry. *Earth Planet. Sci. Lett.* **8**, 448-450.
- SMITH, J. V. (1969) Crystal structure and stability of the MgSiO₃ polymorphs; physical properties and phase relations of Mg, Fe pyroxenes. *Mineral. Soc. Amer. Spec. Pap.* **2**, 3-29.
- (1970) Physical properties of order-disorder structures with especial reference to feldspar minerals. *Lithos*, **3**, 145-160.

- SMYTH, J. R. (1969) Orthopyroxene-high-low clinopyroxene inversions. *Earth Planet. Sci. Lett.* **6**, 406-407.
- (1970) High-temperature single-crystal X-ray studies of natural orthopyroxenes. (abstr.) *Amer. Mineral.* **55**, 312.
- (1972) A simple heating stage for single-crystal diffraction studies up to 1000°C. *Amer. Mineral.* **57**, 1305-1309.
- , AND C. W. BURNHAM (1972) The crystal structures of high and low clinohypersthene. *Earth Planet. Sci. Lett.* **14**, 183-189.
- TAKEDA, H. (1972) The crystallography of some aluminous orthopyroxenes of high pressure origin. *J. Geophys. Res.* **77**, 5798-5811.
- THOMPSON, J. B. (1970) Geometrical possibilities for amphibole structures: model biopyriboles. *Amer. Mineral.* **55**, 292-293.
- VIRGO, D., AND S. S. HAFNER (1969) Fe²⁺, Mg order-disorder in heated orthopyroxenes. *Mineral. Soc. Amer. Spec. Pap.* **2**, 67-81.
- , AND ——— (1970) Fe²⁺, Mg order-disorder in natural orthopyroxenes. *Amer. Mineral.* **55**, 201-223.
- WARREN, B. E., AND D. I. MODELL (1930) The structure of enstatite, MgSiO₃. *Z. Kristallogr.* **75**, 1-14.

*Manuscript received, November 3, 1972;
accepted for publication, December 29, 1972.*